Diffusion-Guided Quantitative Susceptibility Mapping

Amanda C. L. Ng[1,2], David K. Wright[3,4], Parnesh Raniga[2,5], Stephen Moore[6], Gary F. Egan[2], and Leigh A. Johnston[4,7]

[1]Dept of Electrical & Electronic Engineering, The University of Melbourne, Melbourne, VIC, Australia, [2]Monash Biomedical Imaging, Monash University, Melbourne, VIC, Australia, [3]Centre for Neuroscience, The University of Melbourne, Melbourne, VIC, Australia, [4]Florey Institute of Neuroscience and Mental Health, The University of Melbourne, VIC, Australia, [5]The Australian e-Health Research Centre-BioMedIA The Australian e-Health Research Centre-BioMedIA, CSIRO Preventative Health National Research Flagship ICTC, Herston, QLD, Australia, [6]IBM Research Collaboratory for Life Sciences-Melbourne, Victorian Life Sciences Computing Initiative, The University of Melbourne, VIC, Australia, [7]NeuroEngineering Laboratory, Dept. Electrical & Electronic Engineering, The University of Melbourne, Melbourne, VIC, Australia

Target audience Researchers investigating magnetic resonance phase imaging and susceptibility mapping.

Purpose Quantitative susceptibility mapping (QSM) aims to derive reliable estimates of the magnetic susceptibility of voxels from phase data arising from 3D gradient-echo MRI acquisitions. Current approaches model every voxel as a sphere[1-3], however research has demonstrated that white matter voxels are better modeled as cylinders[4]. We propose a new approach to QSM that uses diffusion-weighted MRI to guide geometric model selection in each voxel. We demonstrate that the diffusion-guided QSM method (dQSM) is more accurate and robust than conventional methods.

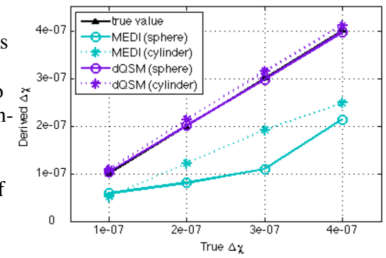

Figure 1 Derived Δχ for numerical phantom.

Methods

Theory ΔB is calculated from T_2* GRE phase data according to $\Delta B = -\gamma.\mathrm{TE}.\phi^{-1}$, where γ is the gyromagnetic ratio of water, TE is echo time and ϕ is phase. The susceptibility map, Δχ, is related to ΔB according to $\Delta B(\boldsymbol{r}) = \sum F(\boldsymbol{r}', \boldsymbol{r}-\boldsymbol{r}')\,\Delta\chi$, where $F(\boldsymbol{r}', \boldsymbol{r}-\boldsymbol{r}') = F_s(\boldsymbol{r}-\boldsymbol{r}')$ for spherically modeled voxels and $F(\boldsymbol{r}', \boldsymbol{r}-\boldsymbol{r}') = F_c(\boldsymbol{r}-\boldsymbol{r}')$ for cylindrically modeled voxels. The spherical kernel function is given by

$$F_S(\boldsymbol{r}) = \begin{cases} \frac{B_0}{4\pi}\left(\frac{3\cos^2\theta - 1}{r^3}\right), & r > 0 \\ 0, & r = 0 \end{cases} \tag{1}$$

where $r = |\boldsymbol{r}|$, θ is the angle between $\boldsymbol{r}$ and B_0 field direction, $\boldsymbol{z}$. The analytical cylindrical kernel function is 2-dimensional, where the plane in which it is defined is normal to the cylinder axis, $\boldsymbol{c}$. The discrete 3D cylindrical kernel function is defined as

$$F_C(\boldsymbol{r}) = \begin{cases} \frac{B_0}{6}\left(3\cos^2\beta - 1\right), & r = 0 \\ P(\boldsymbol{r})\,\frac{1}{2\pi}B_0\frac{1}{r^2}\sin^2\beta\cos 2\varphi, & r > 0 \end{cases} \tag{2}$$

where φ is the angle between the projection of $\boldsymbol{r}$ and $\boldsymbol{z}$ onto the plane normal to $\boldsymbol{c}$, β is the angle between $\boldsymbol{c}$ and $\boldsymbol{z}$. The proportionality function

$$P(\boldsymbol{r}) = \frac{(2\alpha - \boldsymbol{r}\cdot\boldsymbol{c})^2(\alpha + \boldsymbol{r}\cdot\boldsymbol{c})}{4\alpha^3}, \alpha = 0.47 \tag{3}$$

facilitates the discretisation of the analytical kernel, where α was determined computationally to optimise the discrete approximation of the continuous kernel. Fractional anisotropy (FA) and primary eigenvector (V1) maps are calculated from DWI data. Voxels with FA($\boldsymbol{r}'$) < 0.2 are modelled as spheres, while voxels with FA ≥ 0.2 are modelled as cylinders whose axes are defined by V1. Δχ was solved by minimising $\kappa\left\|\mathbf{A}\mathbf{x} - \mathbf{b}\right\|_2^2 + (1-\kappa)\left\|\mathbf{L}\mathbf{x}\right\|_2^2$ where $\mathbf{A}\mathbf{x} - \mathbf{b}$ is the matrix-vector representation of $\sum F(\boldsymbol{r}', \boldsymbol{r}-\boldsymbol{r}')\,\Delta\chi - \Delta B(\boldsymbol{r})$ and $\mathbf{L}$ is a second-order derivative.

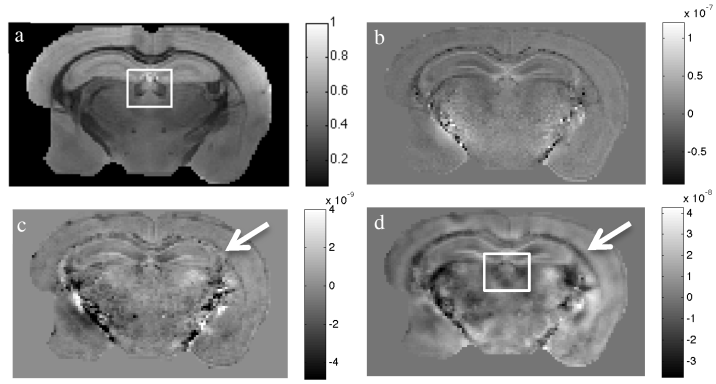

Figure 2 (a) Magnitude, (b) ΔB, (c) MEDI-derived Δχ and (d) dQSM-derived Δχ. Main magnetic field is directed into the page. Squares indicate structures that appear only in the magnitude and dQSM map. Arrows indicate white matter correctly resolved by dQSM.

Simulation Data The dQSM method was applied to a numerical phantom comprising 4 cylinders and 4 spheres paired with matching Δχ of 1e-7, 2e-7, 3e-7 and 4e-7. The cylinder axes were oriented at 90° to the B_0 field. The matrix size was 50×125×75 and radii of cylinders and spheres were 5 voxels.

Experimental Data Ex-vivo mouse brain T_2* GRE (3D EPI, TR=1000ms, TE=100ms, FA = 30°) and DWI (TR=2500ms, TE=65ms, shots=2, δ=3ms, Δ=14ms, 46 dirs, b=1700 s/mm²) data were acquired in a single scan session on a 4.7T Bruker with MTX=192×168×96, voxel size=0.1×0.1×0.1mm³. The GRE magnitude and DWI B_0 images were coregistered using FSL FLIRT. The GRE phase data was unwrapped with ΦUN[5] and filtered with SDF[6].

Computation The Δχ maps were calculated on an IBM BlueGene/Q, taking 16 hours to complete the experimental data maps on 4096 cores. The Landweber iteration was used to compute the minimisations. A lower threshold of 10^{-6} was applied to the kernel values. κ was set to 0.75.

Comparison method MEDI[2]-derived susceptibility maps were computed for comparison. The λ parameter was set to 0.1 based on qualitative analysis of artefact removal and smoothing.

Results

The numerical phantom results (Fig. 1) demonstrate accurate computation of the susceptibility values of the cylinders and spheres for the dQSM method. In contrast, the MEDI method under-estimated the susceptibility values, and computed different values for cylinder-sphere pairs with equal susceptibility. The ex-vivo mouse results (Fig. 2) demonstrate more uniform susceptibility values in the white matter of the corpus callosum (white arrows). Structure visible in the magnitude image (square) is not visible in the MEDI map, but does appear in the dQSM map. The MEDI map appears noisier than the ΔB, while the dQSM map appears less noisy than both MEDI and ΔB.

Discussion

dQSM has demonstrated enhanced ability to resolve Δχ, particularly in the white matter, where cylindrical geometries dominate. While the Δχ values derived by MEDI are known to scale with the regularisation weighting[2], dQSM shows invariance and accuracy of the estimated Δχ values. The main drawback of the proof-of-principle dQSM method is the high computational costs. Current QSM methods that apply only a spherical kernel can invoke the convolution theorem, thereby substantially reducing computation time to Nlog(N) by employing the Fourier transform. Since dQSM involves spatially dependent kernels, the convolution theorem is no longer applicable and computation time is high at N^2. Current work is underway to increase the efficiency of the dQSM approach.

Conclusions

We have demonstrated that using diffusion weighted MRI to guide the selection of cylindrically modelled voxels increases the accuracy of estimated susceptibility values. Our proof-of-concept dQSM method, while computationally expensive, provides a first step beyond the Lorentz sphere model assumption.

References **1.** Liu T, Spincemaille P, Rochefort L de, Kressler B, Wang Y. Calculation of susceptibility through multiple orientation sampling (COSMOS): A method for conditioning the inverse problem from measured magnetic field map to susceptibility source image in MRI. *Magn Reson Med.* 2009;61(1):196–204. **2.** Liu T, Liu J, de Rochefort L, et al. Morphology enabled dipole inversion (MEDI) from a single-angle acquisition: Comparison with COSMOS in human brain imaging. *Magnetic Resonance in Medicine*. 2011;66(3):777–783. **3.** Shmueli K, Zwart JA de, Gelderen P van, et al. Magnetic susceptibility mapping of brain tissue in vivo using MRI phase data. *Magn Reson Med.* 2009;62(6):1510–1522. **4.** Lee J, Shmueli K, Kang B-T, et al. The contribution of myelin to magnetic susceptibility-weighted contrasts in high-field MRI of the brain. *NeuroImage*. 2012;59(4):3967–3975. **5.** Witoszynskyj S, Rauscher A, Reichenbach JR, Barth M. Phase unwrapping of MR images using [Phi]UN - A fast and robust region growing algorithm. Medical Image Analysis. 2009;13(2):257–268. **6.** Ng A, Johnston L, Chen Z, et al. Spatially dependent filtering for removing phase distortions at the cortical surface. Magnetic Resonance in Medicine. 2011;66(3):784–793.